Quaternary Science Reviews 28 (2009) 1941–1955

Contents lists available at ScienceDirect

Quaternary Science Reviews

journal homepage: www.elsevier.com/locate/quascirev

Late Holocene (0–2.4 ka BP) surface water temperature and salinity variability, Feni Drift, NE Atlantic Ocean

T.O. Richter[a,*], F.J.C. Peeters[b], T.C.E. van Weering[a,b]

[a] Department of Marine Geology, Royal Netherlands Institute for Sea Research (NIOZ), P.O. Box 59, 1790 AB Den Burg, Texel, The Netherlands
[b] Department of Marine Biogeology, Faculty of Earth and Life Sciences (FALW), VU University Amsterdam, De Boelelaan 1085, 1081 HV Amsterdam, The Netherlands

ARTICLE INFO

Article history:
Received 14 August 2008
Received in revised form
27 March 2009
Accepted 13 April 2009

ABSTRACT

Planktonic foraminiferal Mg/Ca ratios and oxygen isotopic compositions of a spliced sediment record from Feni Drift, NE Atlantic Ocean (box core M200309 and piston core ENAM9606) trace late Holocene sea surface temperature (SST) and salinity changes over the past 2400 years. At this location, the variability of SST and oxygen isotopic composition of seawater ($\delta^{18}O_w$) reflects variable northward advection of warm and saline surface waters, which appears linked to climate variability over the adjacent European continent. Our records reveal a general long-term cooling trend. Superimposed on this overall trend, partly higher temperatures and salinities from 180 to 560 AD and 750 to 1160 AD may be ascribed to the Roman and Medieval Warm Periods, respectively. Subsequently, our record displays highly variable surface water conditions; the main Little Ice Age SST minimum is restricted to the 15th and 16th centuries AD. Pervasive multidecadal- to centennial-scale variability throughout the sedimentary proxy records can be partly attributed to solar forcing and/or variable heat extraction from the surface ocean caused by shifts in the prevailing state of the North Atlantic Oscillation (NAO). High salinities in the 17th and 18th centuries are considered to reflect tropical anomalies linked to a southward shift of the Intertropical Convergence Zone, propagating across the North Atlantic Ocean.

1. Introduction

Proxy reconstructions of climate change over the past two millennia can constrain the range of natural climate variability prior to the onset of major anthropogenic greenhouse gas emissions. As such, they help to put modern climate change in a longer-term context, and to separate between anthropogenic induced and natural climate variability. Warm and cold intervals of the late Holocene are commonly referred to as the Roman and Medieval Warm Periods vs. Dark Ages and Little Ice Age, respectively. However, these terms may be considered simplistic and therefore misleading (Jones and Mann, 2004), because none of these periods are characterized by sustained warm or cold conditions over several centuries, while peak climate anomalies in individual site-specific records were not synchronous on a global scale. Consequently, such anomalies are less pronounced in hemispheric mean climate reconstructions, and there is no clear definition on the precise timing of the presumed main late Holocene climate fluctuations.

The northward advection of warm and saline surface waters in the North Atlantic towards higher latitudes plays a key role in modulating the Atlantic thermohaline meridional overturning circulation (AMOC), and the related northward heat flux maintains the comparatively mild climate of Europe with respect to the zonal mean. Accordingly, surface water reconstructions along these surface current flow paths have clear implications for European climate variability.

Rockall Trough constitutes one such passageway for inflow of Atlantic waters into the Nordic Seas; Feni Drift at its western margin provides expanded sedimentary sequences to obtain proxy records of past hydrographic changes at high temporal resolution. Proximity of the area to the European continent permits comparison of marine paleorecords with terrestrial climate reconstructions from adjacent areas.

The Mg/Ca ratio in foraminiferal calcite is now an established proxy for past sea surface temperature (SST). Compared to other widely used temperature proxies (alkenone unsaturation ratios, faunal transfer functions), Mg/Ca has the advantage that it is measured on the same phase as foraminiferal oxygen isotopes ($\delta^{18}O_c$). Thus the two records can be used in conjunction to separate temperature effects on $\delta^{18}O_c$ from changes in the oxygen isotopic composition of seawater ($\delta^{18}O_w$) and to infer past surface salinity

* Corresponding author. Tel.: +31 222 369 394; fax: +31 222 319 674.
E-mail addresses: thomasr@nioz.nl (T.O. Richter), frank.peeters@falw.vu.nl (F.J.C. Peeters), tjeerd@nioz.nl (T.C.E. van Weering).

0277-3791/$ – see front matter
doi:10.1016/j.quascirev.2009.04.008

(SSS) changes from reconstructed $\delta^{18}O_w$. Previous downcore applications of the Mg/Ca SST proxy are predominantly from tropical, subtropical and subantarctic sites (see reviews by Lea, 2003; Barker et al., 2005). Only more recently, the Mg/Ca SST proxy was applied to sites from high northern latitudes (Nyland et al., 2006; Peck et al., 2006, 2008; Came et al., 2007; Farmer et al., 2008; Thornalley et al., 2009). Salinity reconstructions from $\delta^{18}O_w$ generally assume an invariant linear $\delta^{18}O_w$–salinity slope throughout the respective paleorecord, though some studies mention possible deviations from a linear slope related to shifts between different water masses (Pahnke et al., 2003; Lund and Curry, 2006; Nyland et al., 2006).

Here, we present high-resolution (on average bidecadal) planktonic foraminiferal Mg/Ca and stable isotope ($\delta^{18}O_c$) records from Feni Drift, Rockall Trough. Our objective is first to evaluate this proxy approach through comparisons of our primary results with 20th century hydrographic data. Then, we assess late Holocene (0–2.4 ka BP) SST and SSS changes, reflecting variable northward advection of warm and saline surface waters, and identify possible forcing mechanisms and relationships with coeval European continental climate variability.

2. Core location and surface hydrographic setting

A piston core (ENAM9606, 55°39.02′N 13°59.10′W, 2543 m water depth) and a box core (M200309, 55°39.10′N 13°59.13′W, 2548 m) were recovered from virtually the same location at Feni Drift on the western margin of Rockall Trough, NE Atlantic Ocean (Fig. 1). The most recent sediments were not retrieved in the top of the piston core, hence the two cores were spliced to extend the record to the present day and to compare proxy results with 20th century hydrographic data.

Rockall Trough (RT) represents one pathway for advection of warm and saline North Atlantic upper water into the Nordic Seas, where these waters are subsequently converted into southward flowing deep overflow waters by thermohaline overturning. Surface waters in the area are derived from two separate source regions (van Aken and Becker, 1996; Hansen and Østerhus, 2000; Holliday et al., 2000). From the southeast, the Continental Slope Current carries Eastern North Atlantic Water (ENAW) formed along the Iberian Peninsula and in the Bay of Biscay. From the southwest, one branch of the North Atlantic Current (NAC) enters RT at least intermittently. This branch is depicted as a continuous current by some authors (Fratantoni, 2001; Orvik and Niiler, 2002), but was not observed in other basinwide studies (Reverdin et al., 2003; Pollard et al., 2004). As subtropical source waters of the NAC have undergone extensive mixing with water of subpolar origin along the current flow path (e.g. Hansen and Østerhus, 2000), NAC-derived waters in RT are relatively cool and fresh with respect to ENAW. For the same reason, the influence of ENAW generally renders RT surface waters distinctly warmer and more saline than NAC-derived waters of the Iceland Basin west of Rockall Plateau.

Seasonal changes in upper ocean hydrography reflect deep winter mixing leading to near-homogenous temperature and salinity down to 500–800 m, followed by the gradual development of upper layer stratification and a seasonal thermocline in spring and summer (e.g. Holliday et al., 2000). Interannual temperature and salinity variability observed in instrumental records is mostly related to the varying influence of ENAW vs. NAC-derived surface waters, linked to regional-scale changes in the extent of the subpolar and subtropical gyres (Bersch, 2002; Holliday, 2003; Hátún et al., 2005). Changing properties of source waters may also play a role, notably during "Great Salinity Anomalies" (Dickson et al., 1988; Belkin et al., 1998) when surface salinities were reduced throughout the subpolar gyre, partly as a result of enhanced freshwater and sea ice input from the Arctic Ocean. On the other hand, effects of local air–sea interaction have negligible if any influence on interannual surface water variability (Holliday, 2003).

Hadley Centre gridded sea surface temperature (SST) data (Rayner et al., 2003) illustrate interannual and interdecadal surface ocean variability at the core site, which is compared to North Atlantic oscillation (NAO) reconstructions (Luterbacher et al., 1999) to assess links with regional patterns of atmospheric variability (Fig. 2). Annual mean SST data are shown in the figure, but individual months display generally similar patterns (see Fig. 6 below). Both datasets are only weakly correlated for individual years ($r^2 = 0.12$, scatter plot not shown), but display a general antiphase relationship if smoothed on decadal timescales relevant to the present study (i.e., comparable to the temporal resolution of the paleorecord and age integration of individual samples, cf. Section 4). Interestingly, SST appears to lead NAO phase shifts on decadal timescales; maximum correlation between both datasets occurs for an SST lead of three years (Fig. 2d). Accordingly, surface ocean variability may induce, rather than respond to patterns of atmospheric variability (cf. Meeker and Mayewski, 2002).

Comparisons between local SST and the instrumental NAO record of Hurrell (1995) (not shown) yield similar results for decadally smoothed data, though here no correlation occurs for annual data ($r^2 = 0.00$). We used the Luterbacher reconstruction for consistency with the remainder of the manuscript (Section 6.5 below).

3. Material and methods

The uppermost 85 cm of the piston core and the entire box core were sliced at 1-cm intervals. Only the top 19 cm of the box core is presented here, excluding data from an underlying burrow inferred from the ^{210}Pb record (see below). About 50–80 individuals of the planktonic foraminifer species *Globigerina bulloides* were hand-picked from the 250 to 315 μm size fraction and subsequently separated into two aliquots for stable isotope and Mg/Ca analyses, respectively.

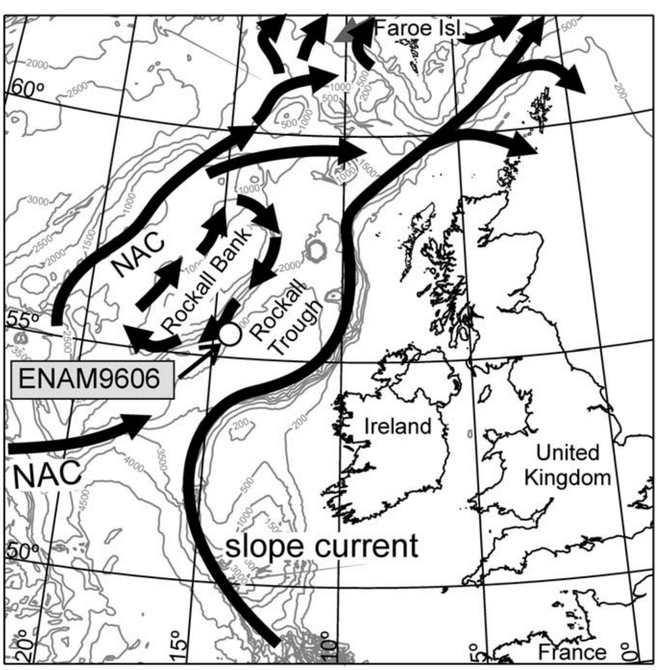

Fig. 1. Core location (white dot) and hydrographic setting. Thick black arrows indicate surface currents; NAC – North Atlantic Current.

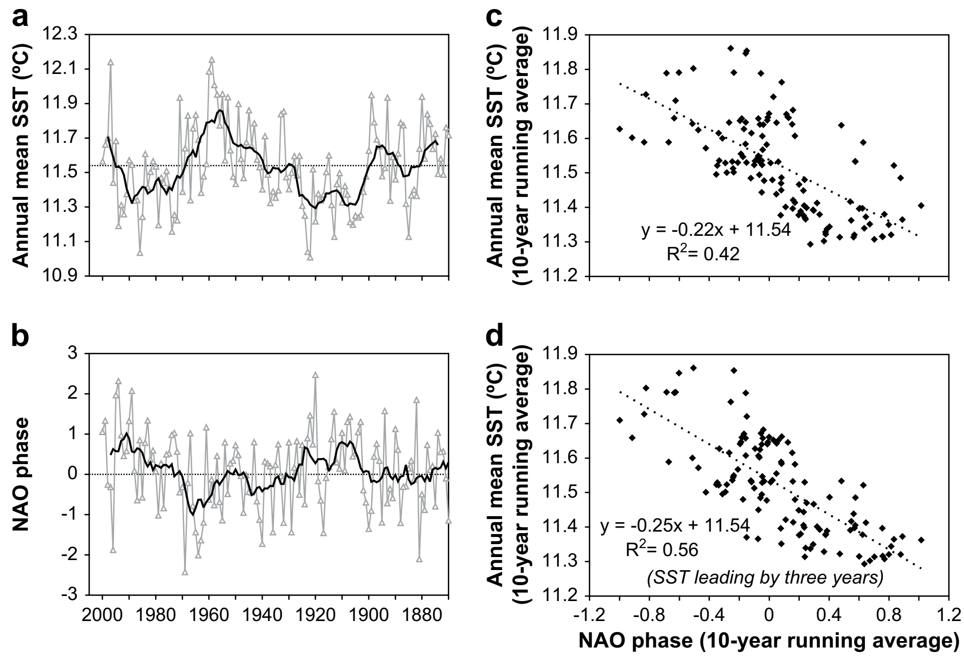

Fig. 2. a) Hadley Centre SST data (Rayner et al., 2003), average values for two grid boxes centered over the ENAM9606 core site. b) North Atlantic Oscillation (NAO) reconstruction (Luterbacher et al., 1999). Bold lines in both panels are 10-point running means [data plotted in panels c) and d)]. Horizontal stippled lines correspond to average SST (11.54 °C) and 'neutral' state of NAO, respectively. c, d) Scatter plots of SST vs. NAO (decadal means in both cases) for c) no lead and d) SST leading by three years.

Stable isotope measurements for the piston core were performed at LSCE Gif sur Yvette using a Finnigan MAT 251 mass spectrometer with an automated Kiel device. All samples were run in duplicate and ~30% in triplicate. Results shown below are the average values of these two or three measurements. Individual analyses typically are comprised of 5–7 shells. Isotopic analyses for the box core were carried out at the VU University Amsterdam on a Finnigan GASBENCH coupled to a Delta+ mass spectrometer. While only three out of nineteen samples were run in duplicate, larger sample sizes (~20 specimens) analyzed on this instrument minimize effects of isotopic variability within the foraminiferal population. All stable isotope results are reported in conventional delta notation versus the Vienna PDB standard (V-PDB); analytical uncertainty for $\delta^{18}O$ is ±0.06‰ for both instruments.

Mg/Ca analyses and sample preparation were carried out at LSCE Gif sur Yvette. 20–30 specimens were cleaned following the method of Barker et al. (2003) to eliminate contamination from clays and organic matter. Magnesium and calcium analyses were performed on a Varian Vista Pro Inductively Coupled Plasma Optical Emission Spectrometer (ICP-OES) according to the procedure described by de Villiers et al. (2002). Precision for measured Mg/Ca ratios determined from replicate runs of a standard solution of Mg/Ca = 5.23 mmol/mol is 0.5% (1σ, RSD). The pooled standard deviation for replicate analysis of *G. bulloides* samples is ±0.17 mmol/mol or ±6.7% (1σ). This is based on 11 replicates, rejecting two duplicate analyses with elevated Mg/Ca (>3 mmol/mol) which possibly reflect incomplete removal of aluminosilicates during the cleaning procedure.

Mg/Ca ratios were converted into calcification temperatures with the species-specific equation of Anand et al. (2003) based on data from Elderfield and Ganssen (2000) ($Mg/Ca = 0.81[\pm0.04]\exp(0.081[\pm0.005] \times SST)$). This equation is based on the cleaning protocol used in this study and was derived from North Atlantic core tops spanning the relevant temperature range. The pooled standard deviation for replicate Mg/Ca analysis corresponds to an uncertainty of ±0.8 °C in temperature reconstructions, comparable to a calibration uncertainty of ±1.2 °C reported by Anand et al. (2003).

Seawater $\delta^{18}O$ ($\delta^{18}O_w$ in ‰ vs. V-SMOW) was estimated from Mg/Ca-derived calcification temperatures and $\delta^{18}O$ of foraminiferal calcite ($\delta^{18}O_c$ in ‰ vs. PDB) by rearranging the isotopic paleotemperature equation of Shackleton (1974) ($T = 16.9 - 4 \times (\delta^{18}O_c - \delta^{18}O_w)$) and solving for $\delta^{18}O_w$. A V-SMOW vs. V-PDB correction of −0.20‰ was applied, consistent with the correction factor common at time of publication of the Shackleton equation (see Bemis et al., 1998). Based on an analytical error of ±0.06‰ for $\delta^{18}O_c$ and a combined analytical and calibration error of ±1 °C for T (Mg/Ca), the uncertainty for reconstructed $\delta^{18}O_w$ is estimated as ±0.26‰.

Other calibration equations were proposed for *G. bulloides* regarding both Mg/Ca (Lea et al., 1999; Mashiotta et al., 1999; Pak et al., 2004; McConnell and Thunell, 2005) and $\delta^{18}O_c$ (Bemis et al., 1998; Peeters et al., 2002; Mulitza et al., 2003). These are however based on different study areas and for Mg/Ca on a different cleaning protocol. For core top samples, all of the above alternative temperature equations would yield calcification temperatures and inferred $\delta^{18}O_w$ values which are inconsistent with the present-day hydrography (cf. below). For our study, use of Shackleton's paleotemperature equation is also justified because Anand et al. (2003) calibrated Mg/Ca against $\delta^{18}O$ calcification temperatures derived with the same equation.

4. Chronology

Eleven accelerator mass spectrometry (AMS) ^{14}C ages were measured at the Utrecht facility on *G. bulloides* (Table 1). Ten ^{14}C dates from the piston core include two minor age reversals which were not considered for the final age model. One date from the box core constrains the splice of proxy records with the 'underlying' piston core (see below). Ages were corrected for a reservoir effect of −400 years and converted into calendar years with the CALIB5.0

Table 1
AMS ^{14}C ages and calibrated (calendar) age equivalents. Depths given are for piston core ENAM9606 unless otherwise indicated. Ages marked by an asterisk (*) were not included in the age model.

Depth (cm)	Uncorrected ^{14}C age	Calendar age [median probability] (1σ age range)	Age AD	UtC reference number
1	746 ± 47	386 (327–437)	1564 (1513–1623)	14120
10	956 ± 45	555 (513–597)	1395 (1353–1437)	11447
20	1043 ± 43	613 (565–651)	1337 (1299–1385)	10996
27.5	1440 ± 100	994 (894–1114)	956 (836–1056)	14121*
35.5	1279 ± 43	824 (776–884)	1126 (1066–1174)	14122
44.5	920 ± 60	530 (479–594)	1420 (1356–1471)	14123*
50	1658 ± 42	1219 (1177–1263)	731 (687–773)	10997
58.5	1820 ± 60	1366 (1289–1417)	584 (533–661)	14124
70	2190 ± 50	1785 (1721–1849)	165 (101–229)	14126
84	2640 ± 60	2328 (2256–2431)	378 (481–306) BC	14125
23.5 (M200309BX)	947 ± 44	548 (504–596)	1402 (1354–1446)	14130

program (Stuiver and Reimer, 1993) and the Marine04 calibration dataset (Hughen et al., 2004).

The age model for the piston core (Fig. 3) is based on a cubic spline (Heegaard et al., 2005) interpolation method using eight AMS age control points. Sedimentation rates are ~25 cm/ka at the base of the studied section prior to ~2 ka BP, and gradually increase thereafter to maximum values of 80–85 cm/ka at 0.6–0.4 ka BP. While we give ages on decadal scales (e.g. 1460 AD) in the results and discussion sections, the precision of the final age model is obviously limited by uncertainties of the individual calendar age equivalents. At 1σ level, these are generally ±50a and higher (+100/−70a) for the base of the record (see Table 1).

In the box core, age control for the last ~150 years is based on radionuclide records (^{137}Cs, ^{210}Pb). Radionuclide analyses were carried out at Royal NIOZ; results are shown in Fig. 4. ^{210}Pb activities were determined for the entire box core by alpha spectrometry indirectly via its granddaughter ^{210}Po; sample preparation followed Boer et al. (2006). Mass accumulation rates were derived from the ^{210}Pb record with a constant flux/constant sedimentation (CF/CS) model fit (Appleby and Oldfield, 1992; Boer et al., 2006). One data point with elevated ^{210}Pb at 20 cm core depth probably corresponds to a burrow and was excluded from the model fit.

To validate the age interpretation of the ^{210}Pb record (cf. Smith, 2001) and to constrain levels of supported ^{210}Pb, ^{137}Cs and ^{226}Ra were analyzed by gamma spectrometry at the top of the box core until ^{137}Cs was no longer detectable in the downcore record. The CF/CS model implies an accumulation rate of 0.0419 g/cm^2 × yr, corresponding to a mean sedimentation rate of ~80 cm/ka for the last 150 years. This result is in close agreement with the ^{137}Cs record, despite low ^{137}Cs activities and consequently large uncertainties. Highest ^{137}Cs activities can be ascribed to the 1986 AD Chernobyl accident, as its instant fallout at the core location exceeded cumulative fallout from nuclear bomb testing by an order of magnitude (Appleby, 2001). The lowermost sample with detectable ^{137}Cs should correspond to the onset of nuclear bomb testing 1953 AD. The CF/CS model fit implies ages of 1987 ± 6 AD and 1949 ± 7 AD, respectively; uncertainties reflect the age integration of the corresponding 1 cm-thick sediment slices. Estimated levels of supported ^{210}Pb are also in close agreement with those inferred from ^{226}Ra in core top samples. Ages below the base of the $^{210}Pb_{excess}$ profile (~1850 AD) are constrained by linear age interpolation to an underlying calibrated AMS ^{14}C date. However, the record was spliced with the piston core record at 19 cm core depth, thus above the inferred burrow.

Sedimentation rates of 25–85 cm/ka combined with a 1 cm sampling resolution result in a temporal resolution of 12–40 years (on average 22 years). As the samples represent adjacent 1 cm-thick sediment slices, the age integration of individual samples is equivalent to the temporal resolution in the respective part of the record.

5. Results

Our late Holocene surface water proxy records are given in Fig. 5, with longer-term trends emphasized by a 3-point running mean line. During the last 2400 years, all records show variability on a range of timescales.

5.1. *Mg/Ca record*

Mg/Ca-derived calcification temperatures vary between 10.1 °C and 15.7 °C. The amplitude of shorter-term fluctuations is generally ~1.5–2 °C, only slightly higher than the calibration uncertainty of ~1 °C for individual data points. Most of these features, however, are robust because temperature peaks and troughs and/or intervening warming/cooling trends are clearly defined by several consecutive observations. The interval from 1150 to 1400 AD, discussed below, may form an exception to this pattern.

The last 2400 years are characterized by an overall long-term cooling trend, also indicated by generally increasing $\delta^{18}O$ values of foraminiferal calcite ($\delta^{18}O_c$). Highest temperatures occur at the base of the record (~350BC) and during the 3rd century AD, lowest ones during the 15th, 16th and 20th centuries AD. Partly higher sea surface temperatures from 180 to 560 AD, 750 to 1160 AD and 1600 to 1800 AD are superimposed on the long-term trend; absolute SST

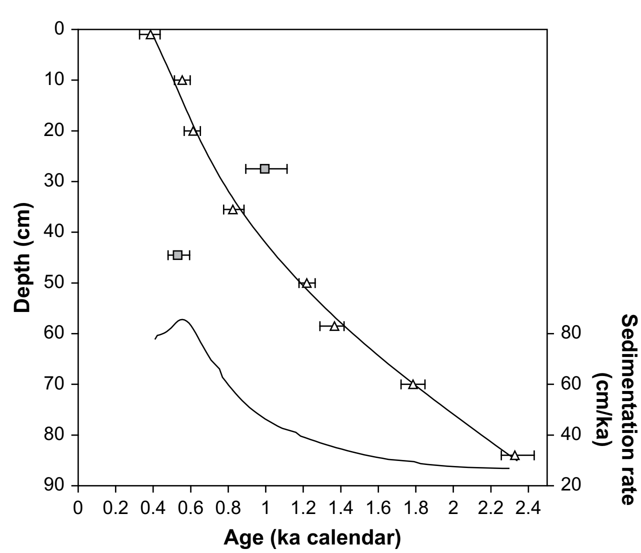

Fig. 3. Age model of piston core ENAM9606. Open triangles: age constraints from ^{14}C dates; grey filled squares: outlier dates omitted from the final age model. Error bars correspond to 1σ uncertainties of calendar age equivalents. Upper curved line is cubic spline fit (Heegaard et al., 2005) through age control points; lower curved line indicates sedimentation rates.

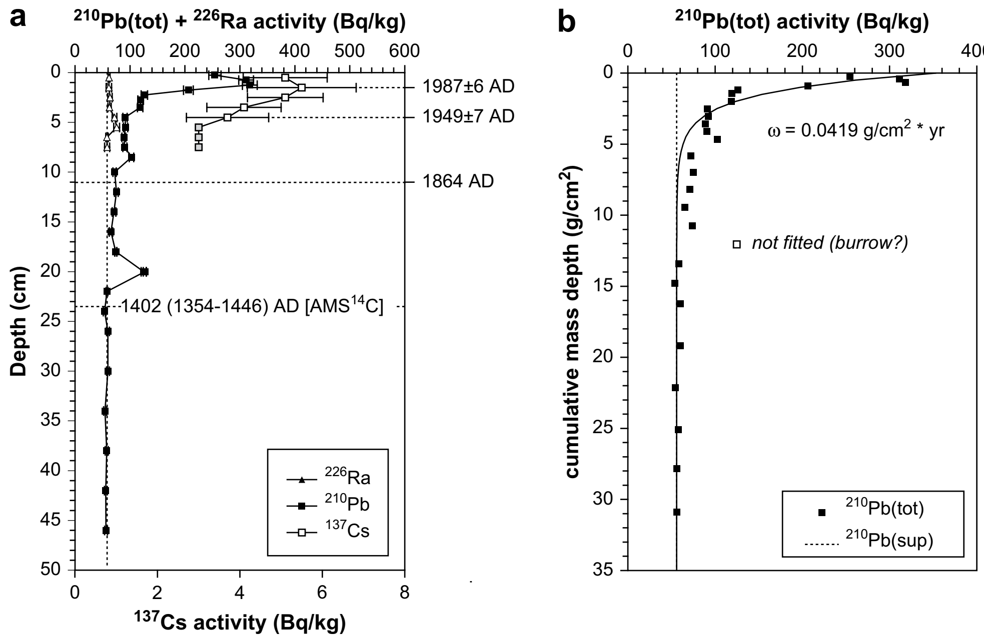

Fig. 4. Radionuclide records for box core M200309BX. a) All data plotted against core depth. Error bars correspond to 1σ uncertainties of activities for the respective isotope (smaller than symbols if not visible). Filled squares at base of ^{137}Cs record represent analyses below the detection limit of 3 Bq/kg. Ages indicated on the right are derived from the constant flux/constant sedimentation (CF/CS) model fit to the ^{210}Pb profile. The two upper ages underline the close agreement with the independent ^{137}Cs tracer (see text). The lowermost age (near the base of the $^{210}Pb_{excess}$ record) corresponds to the switch from ^{210}Pb age control to ^{14}C age control below. b) ^{210}Pb record [same analyses as in panel a)] plotted against cumulative mass depth. Continuous line depicts CF/CS model fit. ^{210}Pb(tot) refers to total ^{210}Pb; ^{210}Pb(sup) represents supported ^{210}Pb in equilibrium with in-situ production from ^{226}Ra.

values tend to become progressively lower for each of these subsequent maxima.

The entire studied period shows pervasive variability on multidecadal to centennial timescales; there are no intervals of sustained stable surface water conditions over several centuries. In particular, the above-mentioned 180–560 AD and 750–1160 AD SST maxima are composed of two or three warm peaks separated by intermittent cooling. Thereafter, the period from 1150 to 1400 AD

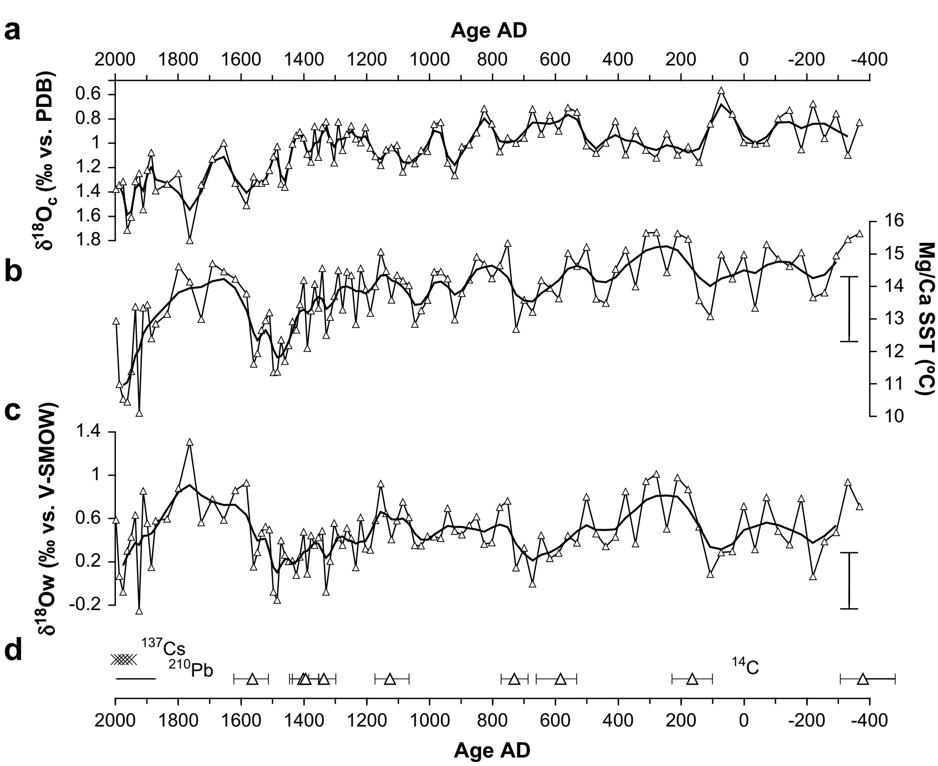

Fig. 5. 0–2.4 ka surface water reconstructions. a) Planktonic oxygen isotope record (*G. bulloides*); b) Mg/Ca sea surface temperature reconstructions; c) oxygen isotopic composition of seawater [derived from a) and b) above]. Thin lines with symbols are raw data in all records; thick line represents 3-point running mean. d) Age control from radionuclide records (^{137}Cs, ^{210}Pb) and AMS ^{14}C ages. Error bars on AMS ages are 1σ uncertainties of calibrated calendar age equivalents.

represents a transitional interval with gradual irregular cooling and particularly pronounced (multi)decadal-scale variability. Here highly unstable surface water conditions imply that *individual* warm and cold 'events' are not always well-defined. A virtually continuous sustained temperature decrease from 1400 to 1485 AD defines the first part of the overall SST minimum during the 15th and 16th centuries. This general temperature minimum also displays an internal "W-shaped structure"; coldest temperatures at ~1500 and ~1560 AD are interrupted by intermittent warming. Pronounced multidecadal variability also occurs during the 20th century.

5.2. Oxygen isotopic composition of seawater ($\delta^{18}O_w$)

The total range in reconstructed $\delta^{18}O_w$ is −0.25 to 1.30‰ vs. V-SMOW. Unlike *T* (Mg/Ca) and $\delta^{18}O_c$, the record does not display a long-term trend. On multicentennial timescales, recurrent shifts occur between periods where $\delta^{18}O_w$ oscillates around mean values of ~0.3–0.45‰ (300 BC–150 AD, 530–730 AD, 1190–1560 AD, 1830–2000 AD) or ~0.55–0.85‰ (180–500 AD, 750–1170 AD, 1580–1800 AD), respectively. Due to superimposed multidecadal variability and the inherent ±0.26‰ uncertainty of the derived $\delta^{18}O_w$ parameter, these periods are to some extent subjectively defined and not always statistically distinguishable from each other.

Generally, higher sea surface temperatures coincide with heavier $\delta^{18}O_w$, implying a positive relationship between temperature and salinity of surface waters. However, transitions in both records are not always precisely synchronous, most notably from 1200 to 1500 AD: here, $\delta^{18}O_w$ displays a gradual and irregular decrease, while the main continuous SST shift occurs only after 1400 AD. Yet both records reach a minimum by 1500 AD.

The foraminiferal oxygen isotope record is variably affected by temperature and salinity effects. For example, $\delta^{18}O_c$ displays relatively heavy values compared to the surrounding time intervals from 150 to 500 AD. As SST maxima occur during the same period, $\delta^{18}O_c$ here dominantly reflects salinity changes.

6. Discussion

6.1. 20th century record and validation against instrumental data

6.1.1. Mg/Ca SST record

Fig. 6 compares Mg/Ca-derived calcification temperatures to the decadally smoothed 20th century instrumental record (Rayner et al., 2003). A previous study inferred that *G. bulloides* proxy records primarily reflect conditions during the northward migrating spring bloom in the North Atlantic (Ganssen and Kroon, 2000). Consistent with results of these authors, our data suggest two main calcifying periods in April/May and June/July, respectively. Obviously these are preferred periods or weighted averages for the entire foraminiferal population, not ruling out calcification of individual specimens during other months or seasons. These seasonal shifts may be related to decadal-scale variability in characteristics and especially timing of the spring bloom (Edwards et al., 2001; Waniek, 2003; Henson et al., 2009). In particular, the increase in Mg/Ca-derived temperatures from the 1960s to the 1990s, implying a seasonal shift from April to June, is fully consistent with the gradually later onset of the North Atlantic subpolar spring bloom over the same time interval inferred by Henson et al. (2009, their Fig. 4).

Shifts in the main calcifying season of *G. bulloides* could also affect earlier parts of our proxy record, but the main features of our SST reconstruction on centennial and longer timescales are largely consistent with commonly assumed patterns of late Holocene

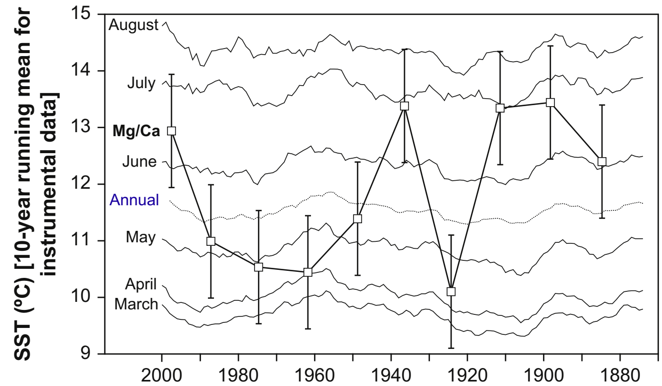

Fig. 6. Comparison of Mg/Ca-derived SST reconstruction with the Hadley Centre instrumental record (Rayner et al., 2003). Running decadal mean plotted for instrumental record, note that March is the coldest month at the core site.

climate variability (see below). Moreover, reconstructed SSTs in parts of our paleorecord (particularly before 1000 AD) exceed 15 °C and are thus higher than 20th century peak summer (August) temperatures. This could indicate that calcification of *G. bulloides* was restricted to peak summer conditions or even individual years with particularly warm summers. Such a scenario was recently proposed for the Younger Dryas (Farmer et al., 2008), but appears unlikely for the late Holocene. We therefore conclude that parts of our SST reconstruction reflect truly warmer SSTs in the past, and shifts in seasonal production of *G. bulloides* represent at least not the dominant control on our paleorecord.

6.1.2. Oxygen isotopic composition of seawater ($\delta^{18}O_w$)

We applied the GEOSECS-based $\delta^{18}O_w$–salinity regression ($\delta^{18}O_w = -19.264 + 0.558\ S$) for North Atlantic surface waters (cf. Duplessy et al., 1991) to test if past salinities can be reconstructed from our derived $\delta^{18}O_w$ values. The 0.26‰ uncertainty for $\delta^{18}O_w$ (cf. above) corresponds to an uncertainty of ~±0.5‰ for reconstructed salinities using the above equation. Fig. 7 shows 20th century salinity reconstructions compared with hydrographic data (www.ices.dk). Our proxy reconstruction qualitatively traces known patterns of North Atlantic multidecadal variability, with cool and partly fresh conditions during the 1920s and 1960s–1970s.

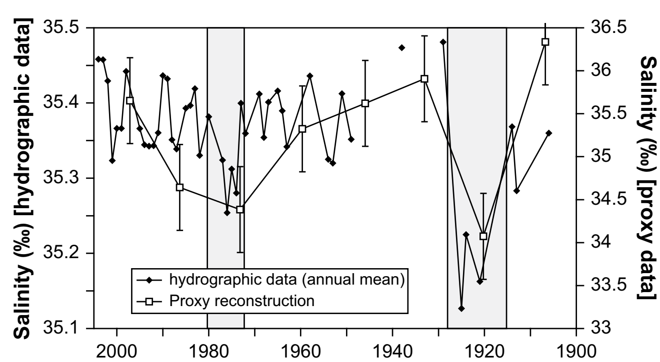

Fig. 7. 20th century $\delta^{18}O_w$ record compared to hydrographic data (www.ices.dk) for the 1° × 1° grid box centered over the core site. Open squares: proxy record. Reconstructed $\delta^{18}O$ of seawater ($\delta^{18}O_w$) was converted into salinity assuming a linear relationship between both parameters (see text). Filled diamonds: hydrographic data. The proxy record traces historical salinity fluctuations, but overestimates of their amplitude by a factor of ~5 (note different y-axis scales, see text for discussion). Shaded rectangles correspond to low salinities in the 1920s and 1970s (Great Salinity Anomaly).

These oscillations were linked to variability in the oceanic thermohaline circulation (e.g. Delworth and Mann, 2000; Latif et al., 2004; Knight et al., 2005).

The above-mentioned approach however overestimates the amplitude of salinity changes by a factor of ∼5 compared to hydrographic data (note different y-axis scales in Fig. 7). On one hand, $\delta^{18}O_W$ retains its relationship with salinity, implying that subtle late Holocene hydrographic variability can be reconstructed beyond uncertainties from error propagation precisely because related changes appear amplified in the $\delta^{18}O_W$ record. On the other hand, it is clear that the GEOSECS-based $\delta^{18}O_W$–salinity relationship cannot be applied at the present core location.

In Fig. 8, reconstructed $\delta^{18}O_W$ is plotted against salinity inferred from the instrumental record and compared with water column data (Schmidt et al., 1999) from the entire North Atlantic and Nordic Seas (0–80°N). This extensive dataset displays considerable scatter around the GEOSECS regression line. In particular, most low-salinity waters north of 60°N show distinctly lower $\delta^{18}O_W$ and plot well below the regression line. As mentioned above in the section on surface hydrography, such waters intermittently affected the subpolar gyre, particularly during "Great Salinity Anomalies". At our core site, variable mixing of these waters with saline waters derived from lower latitudes can thus account for large changes in $\delta^{18}O_W$ for a relatively limited salinity range of ∼35–35.5‰. Our results are consistent with data from the Vøring Plateau (Nyland et al., 2006), where high amplitude fluctuations of $\delta^{18}O_W$ were also attributed to variable influence of $\delta^{18}O_W$ – depleted Arctic waters.

Taking the 0.26‰ uncertainty for $\delta^{18}O_W$ into account, reconstructed $\delta^{18}O_W$ values at Feni Drift fall within the range of water column data for corresponding salinities of 35–35.5‰ (Fig. 8). These $\delta^{18}O_W$ values appear to reflect mixing of different water masses with distinct initial $\delta^{18}O_W$–salinity slopes, precluding the use of a single invariant $\delta^{18}O_W$–salinity relationship. Quantitative salinity reconstructions therefore cannot be achieved for the late Holocene paleorecord presented in this study. As $\delta^{18}O_W$ remains a valid parameter linked to surface water changes, we still interpret it in terms of salinity changes in the following discussion. The inherent 0.26‰ uncertainty for $\delta^{18}O_W$ precludes interpretation of individual small-scale features. Accordingly, we will focus on centennial-scale patterns and some events with an amplitude exceeding the threshold of 0.26‰.

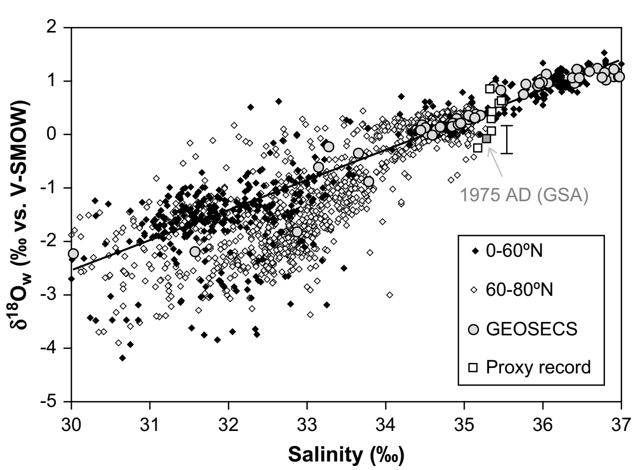

Fig. 8. Reconstructed $\delta^{18}O_W$ plotted against salinity from instrumental record (cf. Fig. 5) and compared with oxygen isotopic measurements of seawater from the North Atlantic and Nordic Seas (0–80°N) (Schmidt et al., 1999). Black line is regression through GEOSECS data points. Proxy sample for 1975 AD ('Great Salinity Anomaly') highlighted; error bar represents ±0.26‰ uncertainty for reconstructed $\delta^{18}O_W$.

6.2. General climatic evolution and comparison with other records

In a "conventional" framework of Late Holocene climate change, the general SST and salinity maxima at 180–560 AD and 750–1160 AD (Fig. 5) might correspond to the Roman and Medieval Warm Periods (RWP and MWP), respectively. However, the onset of the RWP appears delayed with respect to other records; for example, Lamb (1995) defines this interval as ∼0–500 AD. Intermittent climatic deterioration during the "Dark Ages" is suggested in our record by a salinity minimum centered at 600–730 AD. Sea surface temperatures drop during the same interval, but minimum temperatures hardly fall below those of cold spells during the subsequent MWP.

Following the same scheme, the remainder of the record comprises the Little Ice Age (LIA), followed by post-LIA recovery and, possibly, (late) 20th century anthropogenic warming. Several previous studies from the North Atlantic and Norwegian-Greenland Sea provided evidence for considerable surface water variability within the so-called Little Ice Age, commonly including at least two distinct cold spells (e.g. Andersson et al., 2003; Cronin et al., 2003; Knudsen et al., 2004; Nyland et al., 2006; Sicre et al., 2008a,b). Apparent discrepancies in the timing of these cold spells are not discussed here, as it is difficult to assess whether these reflect true spatial variability, divergent results between proxies, or dating uncertainties.

Fig. 9 compares our surface water reconstructions with Greenland ice core data and northern hemispheric temperature reconstructions. At Feni Drift, the salinity drop after ∼1200 AD and the main SST decrease after 1400 AD may represent the onset and early culmination of the LIA, respectively. The salinity decrease coincides with or slightly precedes a temperature decrease over Greenland, interpreted in terms of decreasing North Atlantic Ocean heat transport (Alley et al., 1999). An earlier shift in Greenland temperatures from ∼200–500 AD also concurs with a general salinity and temperature decrease in our marine record. On the other hand, the Greenland temperature record shows little if any superimposed centennial-scale variability over the last 2.4 ka, and has no counterpart for cooler and fresher conditions inferred from our record prior to 200 AD. Comparatively smooth changes in the Greenland temperature reconstruction may result from millennial averaging in this record.

The main SST drop near 1400 AD concurs with a drastic increase in ion concentrations at Summit, Greenland (O'Brien et al., 1995), implying the onset of the LIA as defined by enhanced storminess and changing atmospheric circulation patterns (see also Meeker and Mayewski, 2002). Changing correlation patterns between Feni Drift surface water properties and other circum-North Atlantic climate records (see below) may be related to this pronounced 'regime shift' in hemispheric boundary conditions. The SST drop is also synchronous with a marked decrease in reconstructed northern hemispheric mean temperatures (e.g. Mann and Jones, 2003; see also Jones and Mann, 2004 and references therein; Moberg et al., 2005). Yet there is little similarity between our SST record and hemispheric mean temperatures after ∼1450 AD; the partial apparent antiphase relationship will be discussed below (Section 6.5).

6.3. Solar forcing of centennial-scale variability

Various proxy studies provided empirical evidence for solar forcing of paleoclimate in the North Atlantic and adjacent areas (e.g. Bond et al., 2001; Black et al., 2004; Jiang et al., 2005; Haltia-Hovi et al., 2007). Later modeling questioned the role of solar forcing in modulating climate for the entire Holocene and millennial timescales (Marchal, 2005), while supporting proxy

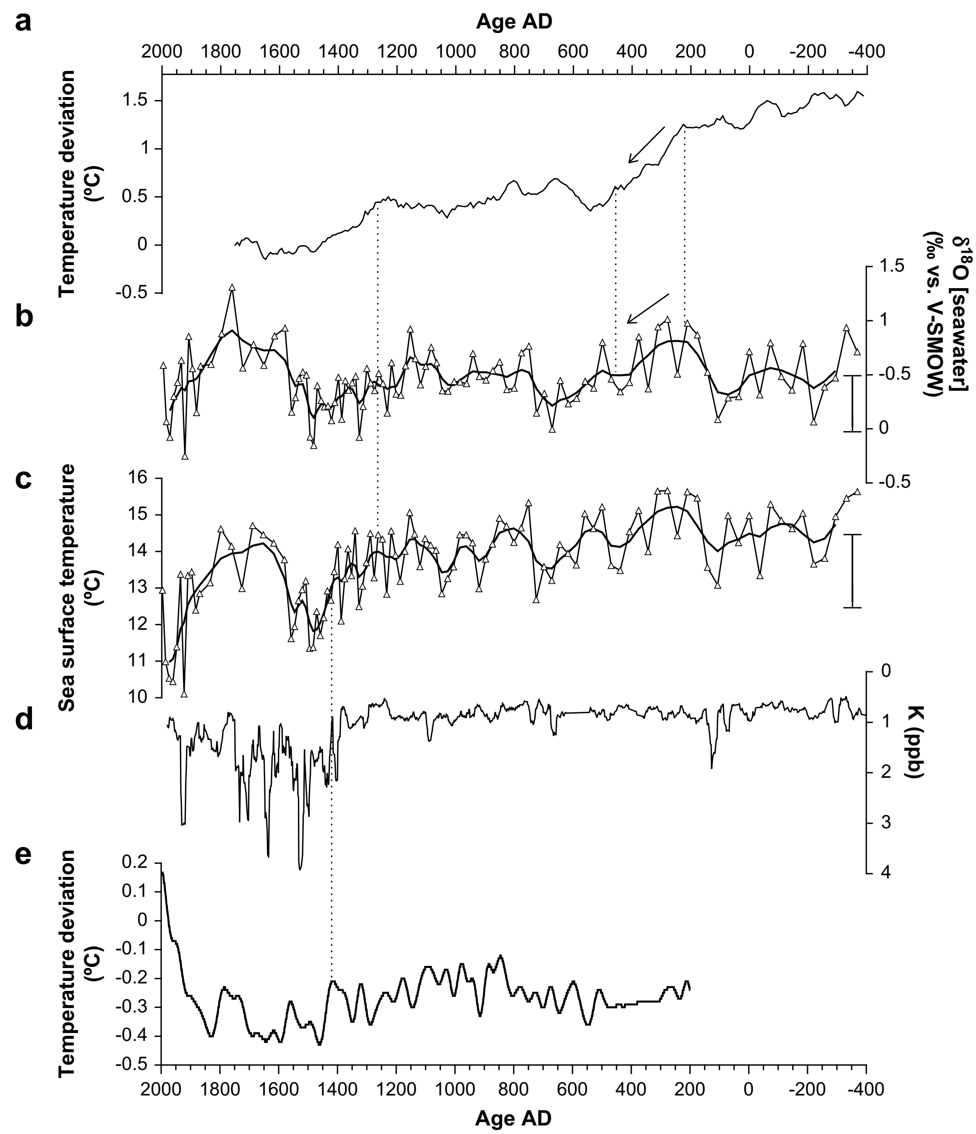

Fig. 9. Comparison of Feni Drift surface water variability with Greenland ice core data and hemispheric temperature reconstructions. a) Greenland annual mean temperature (deviation from top of record at 1750 AD) (Alley et al., 1999); b) and c) Feni drift proxy reconstructions (*this study*); d) GISP ion concentrations, indicating enhanced storminess after ca 1400 AD (O'Brien et al., 1995); e) Northern hemispheric annual mean temperature reconstruction (Mann and Jones, 2003). Stippled vertical lines depict approximately coeval changes in several records (discussed in text).

reconstructions for the last millennium and decadal to centennial timescales (Ammann et al., 2007). However, the climate system also displays internal (unforced) fluctuations, which may equally account for decadal- to centennial-scale variability of surface water properties in our record and could possibly mask a forced response to solar variability (e.g. Goosse et al., 2005; Bengtsson et al., 2006). To assess the role of solar forcing, we compare our late Holocene surface water reconstructions with the residual $\Delta^{14}C$ record of Stuiver et al. (1998) (Fig. 10). In the latter record, maxima in atmospheric ^{14}C correspond to minima in solar activity and vice versa.

The Mg/Ca-derived surface temperature record shows notable similarities with atmospheric ^{14}C concentrations (Fig. 10a). In particular, the SST drop during the 15th and 16th centuries is closely linked to the Spörer Minimum of solar activity, concerning both timing and internal structure. Four earlier well-defined SST minima centered at 440, 730, 920 and 1050 AD also appear to coincide with maxima in the residual $\Delta^{14}C$ record; hence solar forcing can account for the internal structure of the so-called Roman and Medieval Warm Periods and, partly, for intervening cooling during the "Dark Ages". Two other solar activity minima do not have clear counterparts in our SST reconstruction: the SST drop during the Wolf minimum is slightly more sustained, but displays roughly the same amplitude as surrounding 'ambient' multidecadal variability. Cooling during the Maunder minimum appears to be short-lived and not exactly synchronous, conceivably due to relatively low resolution in this part of our paleorecord. Yet the only apparent mismatch between residual $\Delta^{14}C$ and Mg/Ca SSTs occurs near the base of the record, and could be reconciled if ages are shifted by ~100 years (arrow in Fig. 10a), within the 1σ uncertainty of the constraining AMS ^{14}C age.

The overall relationship between residual $\Delta^{14}C$ and the oxygen isotopic composition of seawater (Fig. 10b) is somewhat less clear, but two of the most pronounced inferred salinity drops at 1330 and 1490 AD concur with ^{14}C maxima of the Wolf and Spörer solar activity minima, respectively. In both cases, the peak-to-trough amplitude for $\delta^{18}O_w$ is >0.5‰, thus exceeding the ±0.26‰ error

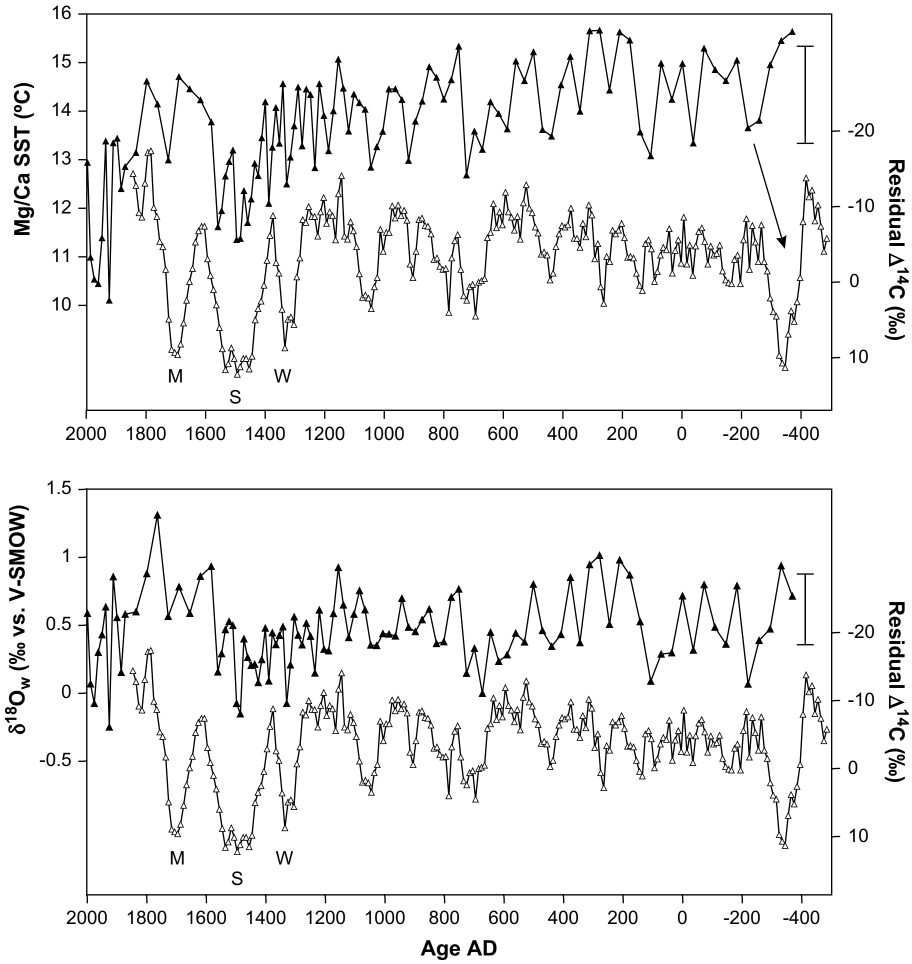

Fig. 10. Comparison of Feni Drift surface water records (filled triangles) with atmospheric residual $\Delta^{14}C$ (open triangles) (Stuiver et al., 1998), indicating variable solar activity. Note inverted scale for $\Delta^{14}C$ to underline general correspondence between reduced solar activity ($\Delta^{14}C$ maxima) and reduced SST and $\delta^{18}O_w$. Arrow depicts tentative correlation at base of record (see text). M, S and W refer to Maunder, Spörer and Wolf minima of solar activity.

derived above. Decreases in $\delta^{18}O_w$ most likely reflect reduced northward advection of saline surface waters, hence changes in the basin-scale meridional overturning circulation.

Consistent with earlier suggestions (Bond et al., 2001), modeling studies indicate that reduced solar irradiance increases the probability of cooling, sea-ice expansion and possibly reduced thermohaline overturning in the Nordic Seas (Goosse and Renssen, 2004; Renssen et al., 2006), providing an oceanic feedback amplifying centennial-scale late Holocene climate variability. On the other hand, such cold events also occur in model simulations with constant forcing and may thus as well result from internal unforced oceanic variability (Hall and Stouffer, 2001; Goosse et al., 2002). High-latitude cooling implies decreased northward oceanic heat transport and will thus affect the entire North Atlantic basin. Cooling may be more pronounced for relatively long-lasting total solar irradiance anomalies (Renssen et al., 2006), which is consistent with the particularly well-defined signature of the Spörer Minimum at Feni Drift.

6.4. *High salinities ~1600–1800 AD: changes in low-latitude source areas*

Patterns of surface water variability during the 17th and 18th centuries, commonly included within the Little Ice Age, may constitute the most surprising part of our records. Temperatures and salinities at least as high as during earlier warm and saline intervals seem to imply strong northward advection of warm and saline surface waters, yet terrestrial records display pronounced cooling over the same period (cf. above). We link the ENAM9606 surface water salinity record to anomalous conditions in the low-latitude source area of the North Atlantic Current (Fig. 11).

Until ~1400 AD, the Feni Drift surface water record displays the expected relationship with Gulf Stream volume transport across the Florida Straits (Lund et al., 2006). Decreasing volume transport may result in reduced oceanic heat and salt fluxes to high northern latitudes, in agreement with gradually declining temperatures and salinities in our record. However, thereafter and particularly after 1600 AD, the opposite relationship occurs: low Gulf Stream volume transport coincides with high temperatures and salinities at our location downstream along the flow path of the North Atlantic Current. During the 17th and 18th centuries, high salinities in our record closely trace elevated salinities at the Dry Tortugas sites southwest of Florida, where surface waters are derived from the tropical Atlantic (Lund and Curry, 2006). Here, high salinities were ascribed to enhanced tropical aridity linked to a southward migration of the Intertropical Convergence Zone (ITCZ). Southward ITCZ migration also led to decreased riverine input and consequently reduced Ti concentration in the Cariaco Basin record of Haug et al. (2001). Salinity changes in our record appear to lag precipitation changes in the Cariaco Basin watershed by ~50 years.

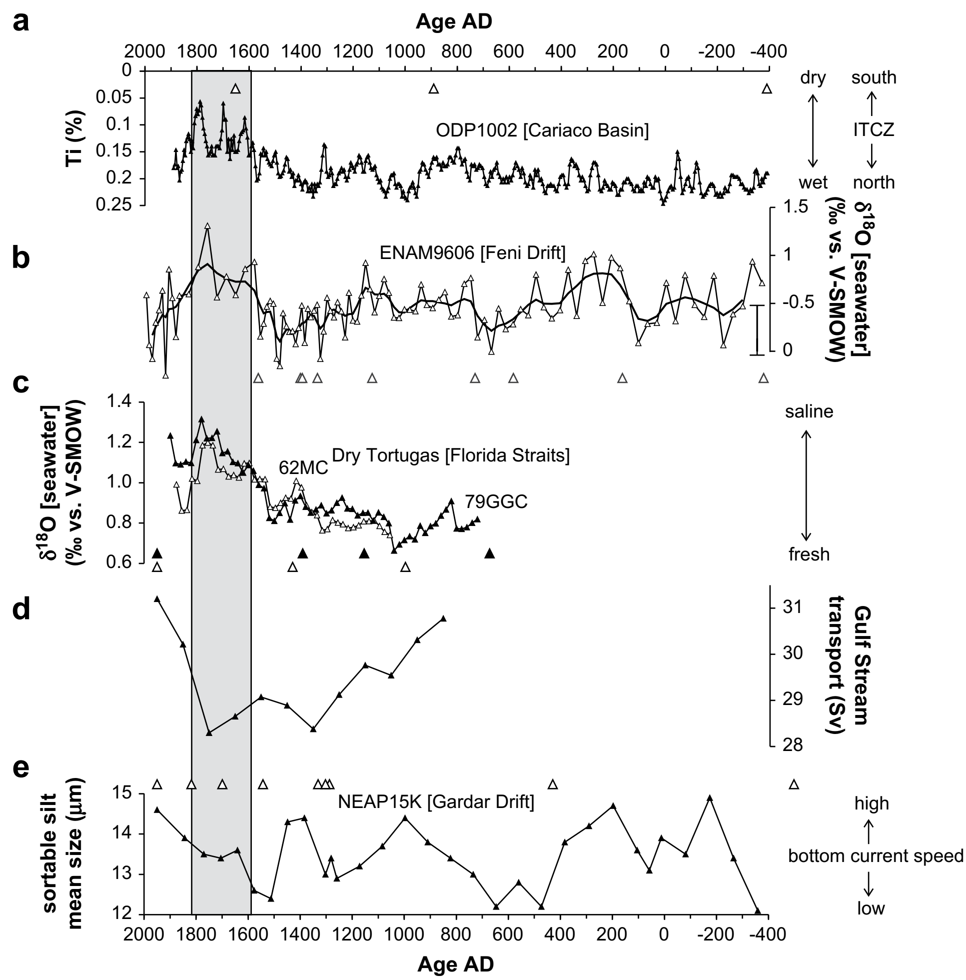

Fig. 11. Link between the high-latitude salinity increase of ∼1600–1800 AD and southward shift of the Intertropical Convergence Zone (ITCZ). a) Cariaco Basin Ti concentration record (Haug et al., 2001) (note inverse scale). Lower Ti concentrations represent enhanced tropical aridity and decreased riverine input. Time scale shifted by 50 years to younger ages (see text). b) Feni Drift oxygen isotopic composition of seawater (*this study*). c) Seawater oxygen isotopic composition at two Dry Tortugas core sites, Florida Straits (Lund and Curry, 2006). d) Reconstructed Gulf Stream transport through Florida Straits (Lund et al., 2006). e) Gardar Drift terrigenous grain-size (Bianchi and McCave, 1999) tracing variable bottom current speed. Shaded rectangle corresponds to maximum southward ITCZ shift with corresponding anomalies in all records shown. Triangles without connecting lines depict AMS age control for each proxy record.

This lag is consistent with modeling results indicating that tropical salinity anomalies propagate towards the subpolar North Atlantic with a lag of 5–6 decades (Vellinga and Wu, 2004). Similar lags cannot be assessed for Florida Strait salinity and transport data discussed above, because the corresponding records shown in Fig. 11 represent 100-year average values.

To facilitate comparisons with our record, the Cariaco Basin timescale is shifted by 50 years to younger ages in Fig. 11a. The abrupt 1560–1580 AD salinity increase at Feni Drift clearly can be linked to an abrupt decrease in Ti concentrations after 1520 AD. Taking our results at face value, three subsequent $\delta^{18}O_w$ maxima at Feni Drift match distinct precipitation minima in the Cariaco Basin record with the same ∼50-year lag. However, this link cannot be rigorously assessed; given the uncertainty of ±0.26‰ for $\delta^{18}O_w$, only the last maximum in our record may be robust.

The shift after ∼1600 AD is closely synchronous in four independently dated records (Haug et al., 2001; Lund and Curry, 2006; this study). Over the interval of overlap, it is the most pronounced anomaly in all three low-latitude records. Coeval ITCZ shifts also occurred over Africa (e.g. Brown and Johnson, 2005); hence associated hydrological changes could also affect the wider source area of the Continental Slope Current. Thus the related salinity signal will be recorded by both surface current branches entering Rockall Trough.

Within the longer-term context (0–14.3 ka BP) provided by the entire Cariaco basin record, similar precipitation minima and inferred southward ITCZ shifts occur only intermittently between ∼3.8 and 2.8 ka BP and continuously during the Younger Dryas. While some of the variability in $\delta^{18}O_w$ at our Feni Drift site prior to 1500 AD could be linked to minor precipitation minima inferred from the Cariaco basin record, the age model of Haug et al. (2001) cannot resolve the precise timing of this centennial-scale variability.

Relatively high LIA salinities were also reconstructed at the Vøring Plateau, Norwegian Sea, and interpreted in terms of decreasing surface water stratification and reduced influence of low-salinity Arctic water masses (Nyland et al., 2006). However, these findings could, at least in part, also be linked to the remote tropical forcing outlined above. Advection of salinity anomalies from the tropics to high northern latitudes will increase surface water densities at convection sites, potentially stabilizing the global thermohaline circulation (e.g. Latif et al., 2000; Vellinga et al., 2002). Indeed, a Gardar Drift grain-size record recording changes in deep-water flow speed (Bianchi and McCave, 1999) displays the main LIA flow anomaly in the 16th century, followed by partial recovery of the thermohaline circulation coinciding with increased surface water salinities (*this study*; Nyland et al., 2006) in subsequent centuries (Fig. 11e).

6.5. Relationship between SST and North Atlantic Oscillation (NAO) phase shifts

The remote tropical forcing mechanism outlined above accounts for high surface salinities during part of the Little Ice Age. While the related stabilization of the thermohaline circulation could also imply a renewed increase in northward oceanic heat flux, comparatively warm sea surface temperatures during the same period seem to contradict pronounced terrestrial cooling in both hemispheric reconstructions (cf. above) and regional European records (Fig. 12).

The entire 17th century AD and the second half of the 18th century are characterized by a predominantly negative state of the winter North Atlantic Oscillation (NAO), with sustained NAO- conditions commonly prevailing over several consecutive

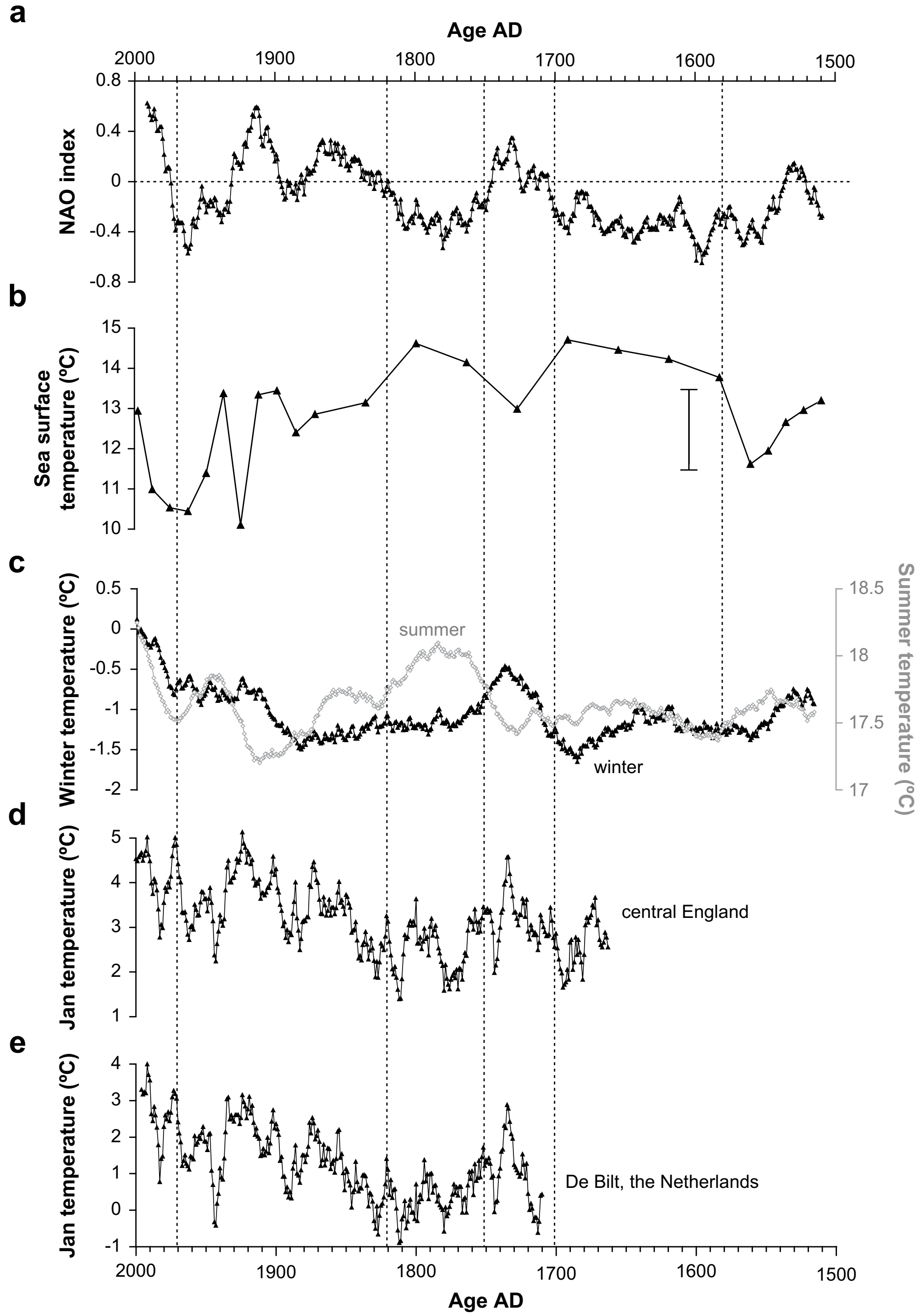

Fig. 12. Variable land–ocean contrast 1600–1800 AD and relationship with North Atlantic Oscillation (NAO) phase shifts. a) NAO reconstructions (20-point running mean) (Luterbacher et al., 1999, 2002). Horizontal line corresponds to 'neutral' state of the NAO. b) Feni Drift sea surface temperature (*this study*). c) Seasonal European temperature reconstructions (30-point running mean) (Luterbacher et al., 2004). d) and e) Instrumental surface air temperature records from central England (Parker et al., 1992, updated by Hadley Centre for Climate Change) and De Bilt, the Netherlands (van Engelen and Nellestijn, 1996, updated by the Dutch Royal Meteorological Institute (KNMI)), both given as 10-point running means. Vertical stippled lines delineate phases of varying land–ocean temperature contrast (see text) and accelerated terrestrial warming after 1970 AD.

winter seasons (Luterbacher et al., 1999, 2002). The core site is located near the hinge point of NAO-related variability (Hurrell, 1995; Rodwell et al., 1999); hence on interannual timescales Rockall Trough surface water variability will not be strongly linked to NAO phase shifts (cf. Holliday et al., 2000). However, relatively sustained NAO- conditions over (multi)decadal timescales may induce opposing temperature trends over the North Atlantic and the adjacent European continent. A negative state of the NAO is consistently characterized by weakened westerly winds, which will lead to decreased heat extraction from the Atlantic Ocean and colder, more continental winter climate over adjacent land areas, consistent with patterns shown in Fig. 12. Decreased winter mixing of the upper water column may provide an additional mechanism for relatively warm late spring to early summer SSTs in our reconstruction.

Surface Ocean cooling during the first half of the 18th century is defined by a single data point in our record, but consistent with a changing ocean–land climate relationship induced by a dominantly positive phase of the NAO. Winter warming over land is contemporaneously shown by both continental-scale reconstructions and two long instrumental records of surface air temperature (Parker et al., 1992; van Engelen and Nellestijn, 1996). Glacier advances in southern Norway during the same interval were attributed to increased winter precipitation rather than decreased summer ablation, consistent with a prevailing NAO+ phase (Nesje and Dahl, 2003).

During the second half of the 18th century, hemispheric annual mean temperature reconstructions imply relatively mild conditions (see Fig. 9 above). The study of Luterbacher et al. (2004) suggests that this reflects warming during non-winter seasons, particularly in summer. As the NAO is dominantly a wintertime phenomenon, the NAO- induced antiphase relationship between land and ocean temperatures also holds for this part of the record.

Towards the top of our record, the final SST warming trend concurs with distinct continental-scale warming, consistently reaching unprecedented maximum temperatures after ~1990 AD in both summer and winter. The two instrumental records display similar patterns for certain months as well as annual mean temperatures (not shown). Likewise, several hemispheric reconstructions show accelerated warming after 1970 AD. Unlike these disparate datasets, the SST increase over the last three decades does not, or not "yet", appear unusual compared to the entire 0–2.4 ka record. Indeed, the core top SST is still lower than during large parts of the prior record, but agrees with present-day hydrographic data. Consistent with recent observational studies (Hobson et al., 2008; Lozier et al., 2008), it appears that pronounced natural variability in the North Atlantic is masking or dampening global anthropogenic warming. Moreover, the warming trend over the second half of the 20th century has not yet reverted the late Holocene millennial-scale cooling.

NAO- related atmospheric variability may also affect earlier parts of our SST record. The reconstruction of Luterbacher et al. (1999, 2002), based on comprehensive geographic coverage of various predictor datasets, extends to 1500 AD only. For earlier periods, NAO behavior was inferred from site-specific proxy records, hence relying on assumed stationarity in statistical relationships between such proxies and the NAO itself (e.g. Schmutz et al., 2000). Lamy et al. (2006) reconstructed hydrological changes from sedimentary records in the Black Sea and northern Red Sea, and interpreted recurrent shifts and a consistent antiphase relationship between both areas throughout the Holocene in terms of long-term NAO variability. Given the above-mentioned caveat and

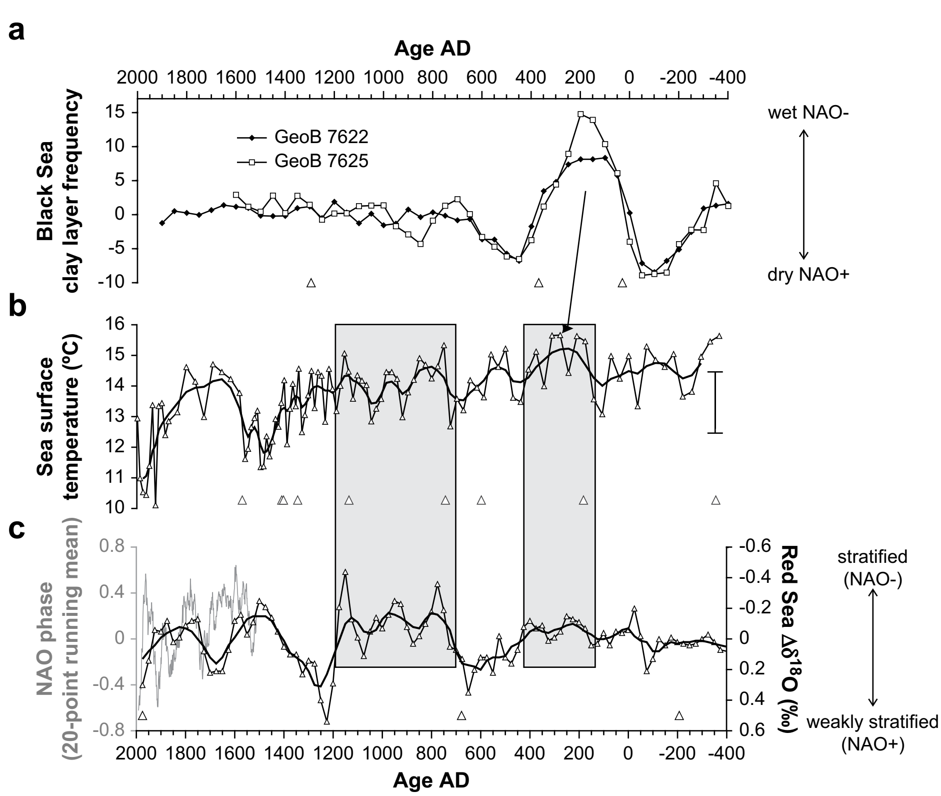

Fig. 13. Comparison of Feni Drift sea surface temperature record with records of hydrological changes in the Black Sea and Red Sea catchment areas, interpreted in terms of NAO teleconnection patterns (Lamy et al., 2006). a) Black Sea clay layer frequency (number of clay layers per 200 years, data detrended and normalized to unit mean). b) Feni Drift Mg/Ca-derived SST record (*this study*), thick black line is 3-point running mean. c) Red Sea stable oxygen isotopic difference between planktonic species *Globigerinoides ruber* (white) and benthic species *Cibicidoides mabahethi* [data detrended and normalized to unit mean, thick black line is 5-point running mean].

chronological uncertainties involved in comparing radiocarbon-dated marine records, our SST record shows interesting similarities with their data (Fig. 13), especially for intervals with nearby AMS age control in the Black Sea and Red Sea records. Hence, NAO phase shifts could also have affected Feni Drift surface water variability prior to 1500 AD.

Within chronological uncertainties, a pronounced maximum in Black Sea clay layer frequency (indicating enhanced riverine input attributed to NAO- conditions) may coincide with the highest SSTs of our record. Thereafter, the Black Sea records show no major variability and, different from earlier parts of these records covering the entire Holocene, little correspondence between the two cores investigated.

During the same interval, the Red Sea record of Lamy et al. (2006) displays a minor but persistent maximum regarding water column stratification ascribed to a persistent NAO- situation by these authors. More strikingly, the "W-shaped" structure ~750–1150 AD is also seen in the Feni Drift SST record. Yet the correlation between both datasets breaks down after 1150 AD, which could conceivably reflect changing NAO teleconnection patterns. However, as the Red Sea age model has no AMS age constraints between 678 AD and the modern core top age, chronological uncertainties in the Red Sea record are a more plausible explanation. In particular, the Red Sea record appears to be inconsistent with the Luterbacher reconstruction over the interval common to both datasets.

7. Summary and conclusions

We presented one of the first high-resolution planktonic foraminiferal Mg/Ca and stable isotope records for the late Holocene of the high-latitude North Atlantic. As the core site is located along one of the main flow paths for northward advection of warm saline surface waters, inferred changes in surface water properties should largely reflect basin-scale ocean circulation changes, in turn affecting climate over the adjacent European continent. On multi-centennial timescales, our records are consistent with commonly assumed patterns of late Holocene climate variability, namely the so-called Roman and Medieval Warm Periods, Dark Ages cooling and Little Ice Age. However, none of these periods were uniformly warm or cold over several consecutive centuries, and the actual causes for this multicentennial variability remain elusive.

On decadal to centennial timescales, we can reasonably ascribe changes in Mg/Ca-derived calcification temperatures to solar forcing and North Atlantic Oscillation (NAO) phase shifts. Both forcing mechanisms are not mutually exclusive, but may represent complementary explanations as exemplified by the "W-shaped structure" of the Medieval Warm Period. Consistent with modeling studies, the surface ocean response to solar forcing appears to be non-linear and partly stochastic, hence variably pronounced for individual solar activity minima. Variable heat extraction from the ocean surface as related to NAO phase shifts can account for divergent temperature patterns over the Atlantic Ocean and the adjacent European continent. These local effects could overprint or modify the primary signal linked to ocean circulation changes; additional high-resolution records along the North Atlantic current flow path would be required to assess the relative importance of basin-scale circulation changes vs. local air–sea exchange.

The rapid southward shift of the Intertropical Convergence Zone (ITCZ) after ~1600 AD is unique for the last 2400 years, and a viable explanation for high $\delta^{18}O_w$ in our data from 1600 to 1800 AD, a period commonly included within the Little Ice Age. We cannot rule out an influence of ITCZ shifts for earlier parts of our record, yet it is plausible that only *major* anomalies in low-latitude source areas will have a *dominant* effect on surface water properties far downstream along the NAC flow path.

The three above-mentioned forcing mechanisms can account for the dominant features of our surface water reconstructions. Additional contributing factors may include internal (unforced) ocean variability, and possibly shifts in seasonal production patterns of *G. bulloides* [cf. Section 6.1.1 above and Farmer et al. (2008)]. From our surface water reconstructions and comparisons with previous results, we draw the following main conclusions:

1. For the Feni Drift core site, the general linear North Atlantic relationship between salinity and $\delta^{18}O$ of seawater does not hold. Instead, $\delta^{18}O_w$ appears to reflect variable mixing of various surface water masses with distinct initial $\delta^{18}O_w$–salinity slopes.
2. Mg/Ca-derived sea surface temperatures indicate a general long-term cooling trend over the last 2.4 ka. Partly higher SSTs and higher salinities from 180 to 560 AD and 750 to 1160 AD might represent the local expression of the Roman and Medieval Warm Periods, respectively. In both cases, however, these warm and saline conditions are not sustained over several centuries.
3. At the core site, the first cold spell of the Little Ice Age occurs ~1400–1570 AD preceded by an irregular salinity decrease starting ~1200 AD. The 17th and 18th centuries display again higher temperatures and salinities. Surprisingly, a second phase with relatively cool and fresh surface water conditions encompasses also most of the 20th century.
4. Pervasive multidecadal- to centennial-scale surface water variability throughout our record can be partly ascribed to solar forcing and/or diminished heat extraction from the surface ocean related to periods with a sustained negative phase of the North Atlantic Oscillation (NAO).
5. High salinities in the 17th and 18th centuries can be linked to a pronounced southward shift of the Intertropical Convergence Zone, followed by propagation of induced salinity anomalies from the tropical to the subpolar North Atlantic.

Acknowledgments

We thank Laurent Labeyrie, Elsa Cortijo and Nicolas Caillon for new data presented in this paper, and Richard Alley, David Lund and Nick McCave for sharing their published data. André Bahr, Gerald Ganssen, Antoon Kuijpers, David Lund, Matthias Moros, Didier Roche, Hendrik van Aken, Gerard van der Schrier, Hans van Tuinen and Heinz Wanner provided comments, suggestions and discussion at various stages of this study. Wim Boer and Rineke Gieles obtained the radionuclide records (^{210}Pb, ^{137}Cs). Instrumental SST data were downloaded from www.metoffice.gov.uk/hadobs. We appreciate constructive comments and suggestions from three anonymous reviewers. This study was supported by the EU-PACLIVA project (Patterns of Climate Variability in the North Atlantic) project (EU EVK2-2002-00143 – T.O.R., T.C.E.v.W.), as well as the Dutch Science Foundation (NWO) funded project VAMOC (854.00.021 – F.J.C.P., T.C.E.v.W.).

References

Alley, R.B., Ágústsdóttir, A.M., Fawcett, P.J., 1999. Ice-core evidence of Late-Holocene reduction in North Atlantic Ocean heat transport. In: Clark, P.U., Webb, R.S., Keigwin, L.D. (Eds.), Mechanisms of Global Climate Change at Millennial Time Scales. Geophys. Monogr. Ser, vol. 112. AGU, Washington, DC, pp. 301–312.

Ammann, C., Joos, F., Schimel, D.S., Otto-Bliesner, B.L., Tomas, R.A., 2007. Solar influence on climate during the past millennium: results from transient simulations with the NCAR climate system model. Proc. Natl. Acad. Sci. USA 104, 3713–3718.

Anand, P., Elderfield, H., Conte, M.H., 2003. Calibration of Mg/Ca thermometry in planktonic foraminifera from a sediment trap time series. Paleoceanography 18 (2), 1050. doi:10.1029/2002PA000846.

Andersson, C., Risebrobakken, B., Jansen, E., Dahl, S.O., 2003. Late Holocene surface–ocean conditions of the Norwegian Sea (Vøring Plateau). Paleoceanography 18 (2), 1044. doi:10.1029/2001PA000654.
Appleby, P.G., 2001. Chronostratigraphic techniques in recent sediments. In: Last, W.M., Smol, J.P. (Eds.), Tracking Environmental Change Using Lake Sediments. Basin Analysis, Coring, and Chronological Techniques, vol. 1. Kluwer Academic Publishers, Dordrecht, the Netherlands, pp. 171–203.
Appleby, P.G., Oldfield, F., 1992. Application of lead-210 to sedimentation studies. In: Ivanovich, M., Harmon, R.S. (Eds.), Uranium Series Disequilibrium, Applications to Earth, Marine and Environmental Sciences. Clarendon Press, Oxford, pp. 731–778.
Barker, S., Greaves, M., Elderfield, H., 2003. A study of cleaning procedures used for foraminiferal Mg/Ca paleothermometry. Geochem. Geophys. Geosyst. 4 (9), 8407. doi:10.1029/2003GC000559.
Barker, S., Cacho, I., Benway, H., Tachikawa, K., 2005. Planktonic foraminiferal Mg/Ca as a proxy for past oceanic temperatures: a methodological overview and data compilation for the Last Glacial maximum. Quaternary Sci. Rev. 24, 821–834.
Belkin, I.M., Levitus, S., Antonov, J.I., Malmberg, S.-A., 1998. "Great Salinity Anomalies" in the North Atlantic. Progr. Oceanogr. 41, 1–68.
Bemis, B.E., Spero, H.J., Bijma, J., Lea, D., 1998. Reevaluation of the oxygen isotopic composition of planktonic foraminifera: experimental results and revised paleotemperature equations. Paleoceanography 13 (2), 150–160.
Bengtsson, L., Hodges, K.I., Roeckner, E., Brokopf, R., 2006. On the natural variability of the pre-industrial European climate. Clim. Dynam. 27, 743–760.
Bersch, M., 2002. North Atlantic Oscillation-induced changes of the upper layer circulation in the northern North Atlantic Ocean. J. Geophys. Res. 107 (C10), 3156. doi:10.1029/2001JC000901.
Bianchi, G.G., McCave, I.N., 1999. Holocene periodicity in North Atlantic climate and deep-ocean flow south of Iceland. Nature 397, 515–517.
Black, D.E., Thunell, R.C., Kaplan, A., Peterson, L.C., Tappa, E.J., 2004. A 2000-year record of Caribbean and tropical North Atlantic hydrographic variability. Paleoceanography 19, PA2022. doi:10.1029/2003PA000982.
Boer, W., van den Bergh, G.D., de Haas, H., de Stigter, H.C., Gieles, R., van Weering, T.C.E., 2006. Validation of accumulation rates in Teluk Banten (Indonesia) from commonly applied ^{210}Pb models, using the 1883 Krakatau tephra as time marker. Mar. Geol. 227, 263–277.
Bond, G., Kromer, B., Muscheler, R., Evans, M.N., Showers, W., Hoffmann, S., Lotti-Bond, R., Hajdas, I., Bonani, G., 2001. Persistent solar influence on North Atlantic climate during the Holocene. Science 294, 2130–2136. doi:10.1126/science.1065680. Published online 15 November 2001.
Brown, E.T., Johnson, T.C., 2005. Coherence between tropical East African and South American records of the Little Ice Age. Geochem. Geophys. Geosyst. 6 (12), Q12005. doi:10.1029/2005GC000959.
Came, R.E., Oppo, D.W., McManus, J.F., 2007. Amplitude and timing of temperature and salinity variability in the subpolar North Atlantic over the past 10 k.y. Geology 35, 315–318.
Cronin, T.M., Dwyer, G.S., Kamiya, T., Schwede, S., Willard, D.A., 2003. Medieval Warm Period, Little Ice Age and 20th century temperature variability from Chesapeake Bay, Global Planet. Change 36, 17–29.
Delworth, T.L., Mann, M.E., 2000. Observed and simulated multidecadal variability in the Northern Hemisphere. Clim. Dynam. 16, 661–676.
de Villiers, S., Greaves, M., Elderfield, H., 2002. An intensity ratio calibration method for the accurate determination of Mg/Ca and Sr/Ca of marine carbonates by ICP-AES. Geochem. Geophys. Geosyst. 3 (1), 1001. doi:10.1029/2001GC000169.
Dickson, R.R., Meincke, J., Malmberg, S.-A., Lee, A.J., 1988. The "Great Salinity Anomaly" in the northern North Atlantic, 1968–1982. Progr. Oceanogr. 20, 103–151.
Duplessy, J.C., Labeyrie, L., Juillet-Leclerc, A., Maitre, F., Duprat, J., Sarnthein, M., 1991. Surface salinity reconstructions of the North Atlantic Ocean during the last glacial maximum. Oceanol. Acta 14, 311–324.
Edwards, M., Reid, P., Plaque, B., 2001. Long-term and regional variability of phytoplankton biomass in the Northeast Atlantic (1960–1995). ICES J. Mar. Sci. 58, 39–49.
Elderfield, H., Ganssen, G., 2000. Past temperatures and δ^{18}O of surface ocean waters inferred from foraminiferal Mg/Ca ratios. Nature 405, 442–445.
Farmer, E.J., Chapman, M.R., Andrews, J.E., 2008. Centennial-scale Holocene North Atlantic surface temperatures from Mg/Ca ratios in *Globigerina bulloides*. Geochem. Geophys. Geosyst. 9 (12), Q12029. doi:10.1029/2008GC002199.
Fratantoni, D.M., 2001. North Atlantic surface circulation during the 1990's observed with satellite-tracked drifters. J. Geophys. Res. 106, 2067–2093.
Ganssen, G.M., Kroon, D., 2000. The isotopic signature of planktonic foraminifera from NE Atlantic surface sediments: implications for the reconstruction of past oceanic conditions. J. Geol. Soc. London 157, 693–699.
Goosse, H., Renssen, H., 2004. Exciting natural modes of variability by solar and volcanic forcing: idealized and realistic experiments. Clim. Dynam. 23, 153–163.
Goosse, H., Renssen, H., Selten, F.M., Haarsma, R.J., Opsteegh, J.D., 2002. Potential causes of abrupt climate events: a numerical study with a three-dimensional climate model. Geophys. Res. Lett. 29 (18), 1860. doi:10.1029/2002GL014993.
Goosse, H., Renssen, H., Timmermann, A., Bradley, R.S., 2005. Internal and forced variability during the last millennium: a model-data comparison using ensemble simulations. Quaternary Sci. Rev. 24, 1345–1360.
Hall, A., Stouffer, R.J., 2001. An abrupt climate event in a coupled ocean–atmosphere simulation without external forcing. Nature 409, 171–174.
Haltia-Hovi, E., Saarinen, T., Kukkonen, M., 2007. A 2000-year record of solar forcing on varved lake sediment in eastern Finland. Quaternary Sci. Rev. 26, 678–689.
Hansen, B., Østerhus, S., 2000. North Atlantic–Nordic sea exchanges. Progr. Oceanogr. 45, 109–208.
Hátún, H., Sandø, A.B., Drange, H., Hansen, B., Valdimarsson, H., 2005. Influence of the Atlantic subpolar gyre on the thermohaline circulation. Science 309, 1841–1844.
Haug, G.H., Hughen, K.A., Sigman, D.M., Peterson, L.C., Röhl, U., 2001. Southward migration of the intertropical convergence zone through the Holocene. Science 293, 1304–1308.
Heegaard, E., Birks, H.J.B., Telford, R., 2005. Relationships between calibrated ages and depth in stratigraphic sequences: an estimation procedure by mixed-effect regression. The Holocene 15, 612–618.
Henson, S.A., Dunne, J.P., Sarmiento, J.L., 2009. Decadal variability in North Atlantic phytoplankton blooms. J. Geophys. Res., 114, C04013. doi:10.1029/2008JC005139.
Hobson, V.J., McMahon, C.R., Richardson, A., Hays, G.C., 2008. Ocean surface warming: the North Atlantic remains within the envelope of previous recorded conditions. Deep-Sea Res. I 55, 155–162.
Holliday, N.P., 2003. Air–sea interaction and circulation changes in the northeast Atlantic. J. Geophys. Res. 108 (C8), 3259. doi:10.1029/2002JC001344.
Holliday, N.P., Pollard, R.T., Read, J.F., Leach, H., 2000. Water mass properties and fluxes in the Rockall Trough, 1975–1998. Deep-Sea Res. I 47, 1303–1332.
Hughen, K.A., Baillie, M.G.L., Bard, E., Bayliss, A., Beck, J.W., Bertrand, C.J.H., Blackwell, P.G., Buck, C.E., Burr, G.S., Cutler, K.B., Damon, P.E., Edwards, R.L., Fairbanks, R.G., Friedrich, M., Guilderson, T.P., Kromer, B., McCormac, F.G., Manning, S.W., Bronk Ramsey, C., Reimer, P.J., Reimer, R.W., Remmele, S., Southon, J.R., Stuiver, M., Talamo, S., Taylor, F.W., van der Plicht, J., Weyhenmeyer, C.E., 2004. Marine04 marine radiocarbon age calibration, 26–0 ka BP. Radiocarbon 46, 1059–1086.
Hurrell, J.W., 1995. Decadal trends in the North Atlantic Oscillation: regional temperatures and precipitation. Science 269, 676–679.
Jiang, H., Eiríksson, J., Schulz, M., Knudsen, K.-L., Seidenkrantz, M.-S., 2005. Evidence for solar forcing of sea–surface temperature on the North Icelandic Shelf during the late Holocene. Geology 33, 73–76.
Jones, P.D., Mann, M.E., 2004. Climate over past millennia. Rev. Geophys. 42, RG2002. doi:10.1029/2003RG000143.
Knight, J.R., Allan, R.J., Folland, C.K., Vellinga, M., Mann, M.E., 2005. A signature of natural thermohaline circulation changes in observed climate. Geophys. Res. Lett. 32, L20708. doi:10.1029/2005GL024233.
Knudsen, K.L., Eiriksson, J., Jansen, E., Jiang, H., Rytter, F., Gudmundsdottir, E.R., 2004. Paleoceanographic changes off North Iceland through the last 1200 years: foraminifera, stable isotopes, diatoms and ice rafted debris. Quaternary Sci. Rev. 23, 2231–2246.
Lamb, H.H., 1995. Climate, History and the Modern World. Routledge, New York, 431 pp.
Lamy, F., Arz, H.W., Bond, G.C., Bahr, A., Pätzold, J., 2006. Multicentennial-scale hydrological changes in the Black Sea and northern red Sea during the Holocene and the Arctic/North Atlantic Oscillation. Paleoceanography 21. doi:10.1029/2005PA001184.
Latif, M., Roeckner, E., Mikolajewicz, U., Voss, R., 2000. Tropical stabilization of the thermohaline circulation in a greenhouse warming simulation. J. Clim. 13, 1809–1813.
Latif, M., Roeckner, E., Botzet, M., Esch, M., Haak, H., Hagemann, S., Jungclaus, J., Legutke, S., Marsland, S., Mikolajewicz, U., Mitchell, J., 2004. Reconstructing, monitoring, and predicting multidecadal-scale changes in the North Atlantic thermohaline circulation with sea surface temperature. J. Clim. 17, 1605–1614.
Lea, D.W., 2003. Elemental and isotopic proxies of marine temperatures. In: Elderfield, H. (Ed.), The Oceans and Marine Geochemistry. In: Holland, H.D., Turekian, K.K. (Eds.), Treatise on Geochemistry, vol. 6. Elsevier-Pergamon, Oxford, pp. 365–390.
Lea, D.W., Mashiotta, T.A., Spero, H.J., 1999. Controls of magnesium and strontium uptake in planktonic foraminifera determined by live culturing. Geochim. Cosmochim. Acta 63, 2369–2379.
Lozier, M.S., Ledbetter, S., Williams, R.G., Roussenov, V., Reed, M.S.C., Moore, N.J., 2008. The spatial pattern and mechanisms of heat-content change in the North Atlantic. Science 319, 800–803.
Lund, D.C., Curry, W., 2006. Florida current surface temperature and salinity variability during the last millennium. Paleoceanography 21, PA2009. doi:10.1029/2005PA001218.
Lund, D.C., Lynch-Stieglitz, J., Curry, W.B., 2006. Gulf stream density structure and transport during the past millennium. Nature 444, 601–604.
Luterbacher, J., Schmutz, C., Gyalistras, D., Xoplaki, E., Wanner, H., 1999. Reconstruction of monthly NAO and EU indices back to AD 1675. Geophys. Res. Lett. 26, 2745–2748.
Luterbacher, J., Xoplaki, E., Dietrich, D., Jones, P.D., Davies, T.D., Portis, D., Gonzalez-Rouco, J.F., von Storch, H., Gyalistras, D., Casty, C., Wanner, H., 2002. Extending North Atlantic Oscillation reconstructions back to 1500. Atmos. Sci. Lett. 2, 114–124.
Luterbacher, J., Dietrich, D., Xoplaki, E., Grosjean, M., Wanner, H., 2004. European seasonal and annual temperature variability, trends, and extremes since 1500. Science 303, 1499–1503.
Mann, M.E., Jones, P.D., 2003. Global surface temperatures over the past two millennia. Geophys. Res. Lett. 30 (15), 1820. doi:10.1029/2003GL017184.
Marchal, O., 2005. Optimal estimation of atmospheric ^{14}C production over the Holocene: paleoclimate implications. Clim. Dynam. 24, 71–88.
Mashiotta, T.A., Lea, D.W., Spero, H.J., 1999. Glacial–interglacial changes in Subantarctic sea surface temperatures and δ^{18}O-water using foraminiferal Mg. Earth Planet. Sci. Lett. 170, 417–432.

McConnell, M.C., Thunell, R.C., 2005. Calibration of the planktonic foraminiferal Mg/Ca paleothermometer: sediment trap results from the Guaymas Basin, Gulf of California. Paleoceanography 20, PA2016. doi:10.1029/2004PA001077.

Meeker, L.D., Mayewski, P.A., 2002. A 1400-year high-resolution record of atmospheric circulation over the North Atlantic and Asis. The Holocene 12, 257–266.

Moberg, A., Sonechkin, D.M., Holmgren, K., Datsenko, N.M., Karlén, W., 2005. Highly variable Northern Hemisphere temperatures reconstructed from low- and high-resolution proxy data. Nature 433, 613–617.

Mulitza, S., Boltovskoy, D., Donner, B., Meggers, H., Paul, A., Wefer, G., 2003. Temperature:δ^{18}O relationships of planktonic foraminifera collected from surface waters. Palaeogeogr. Palaeoclimatol. Palaeoecol. 202, 143–152.

Nesje, A., Dahl, S.O., 2003. The 'Little Ice Age' – only temperature? The Holocene 13, 139–145.

Nyland, B., Jansen, E., Elderfield, H., Andersson, C., 2006. *Neogloboquadrina pachyderma* (dex. and sin.) Mg/Ca and δ^{18}O records from the Norwegian Sea. Geochem. Geophys. Geosyst. 7 (10), Q10P17. doi:10.1029/2005GC001055.

O'Brien, S.R., Mayewski, P.A., Meeker, L.D., Meese, D.A., Twickler, M.S., Whintlow, S.I., 1995. Complexity of Holocene climate as reconstructed from a Greenland ice core. Science 270, 962–964.

Orvik, K.A., Niiler, P., 2002. Major pathways of Atlantic water in the northern North Atlantic and Nordic Seas toward Arctic. Geophys. Res. Lett. 29 (19), 1896. doi:10.1029/2002GL015002.

Pahnke, K., Zahn, R., Elderfield, H., Schulz, M., 2003. 340,000-year centennial-scale marine record of Southern Hemisphere climatic oscillation. Science 301, 948–952.

Pak, D.K., Lea, D.W., Kennett, J.P., 2004. Seasonal and interannual variation in Santa Barbara Basin water temperatures observed in sediment trap foraminiferal Mg/Ca. Geochem. Geophys. Geosyst. 5 (12), Q12008. doi:10.1029/2004GC000760.

Parker, D.E., Legg, T.P., Folland, C.K., 1992. A new daily Central England Temperature series, 1772–1991. Int. J. Climatol. 12, 317–342.

Peck, V.L., Hall, I.R., Zahn, R., Elderfield, H., Grousset, F., Hemming, S.R., Scourse, J.D., 2006. High resolution evidence for linkages between NW European ice sheet instability and Atlantic meridional overturning circulation. Earth Planet. Sci. Lett. 243, 476–488.

Peck, V.L., Hall, I.R., Zahn, R., Elderfield, H., 2008. Millennial-scale surface and subsurface paleothermometry from the northeast Atlantic, 55–8 ka BP. Paleoceanography 23, PA3221. doi:10.1029/2008PA001631.

Peeters, F.J.C., Brummer, G.-J.A., Ganssen, G., 2002. The effect of upwelling on the distribution and stable isotope composition of Globigerina bulloides and *Globigerinoides ruber* (planktic foraminifera) in modern surface waters of the NW Arabian Sea, Global Planet. Change 34, 269–291.

Pollard, R.T., Read, J.F., Holliday, N.P., Leach, H., 2004. Water masses and circulation pathways through the Iceland Basin during Vivaldi 1996. J. Geophys. Res. 109, C04004. doi:10.1029/2003JC002067.

Rayner, N.A., Parker, D.E., Horton, E.B., Folland, C.K., Alexander, L.V., Rowell, D.P., Kent, E.C., Kaplan, A., 2003. Global analyses of sea surface temperature, sea ice, and night marine air temperature since the late nineteenth century. J. Geophys. Res. 108 (D14), 4407. doi:10.1029/2002JD002670.

Renssen, H., Goosse, H., Muscheler, R., 2006. Coupled climate model simulation of Holocene cooling events: oceanic feedback amplifies solar forcing. Clim. Past 2, 79–90.

Reverdin, G., Niiler, P.P., Valdimarsson, H., 2003. North Atlantic Ocean surface currents. J. Geophys. Res. 108 (C1), 3002. doi:10.1029/2001JC001020.

Rodwell, M.J., Rowell, D.P., Folland, C.K., 1999. Oceanic forcing of the wintertime North Atlantic Oscillation and European climate. Nature 398, 320–323.

Schmidt, G.A., Bigg, G.R., Rohling, E.J., 1999. Global Seawater Oxygen-18 Database. http://data.giss.nasa.gov/o18data/.

Schmutz, C., Luterbacher, J., Gyalistras, D., Xoplaki, E., Wanner, H., 2000. Can we trust proxy-based NAO index reconstructions? Geophys. Res. Lett. 27, 1135–1138.

Shackleton, N.J., 1974. Attainment of isotopic equilibrium between ocean water and the benthonic foraminifera genus *Uvigerina*: Isotopic changes in the ocean during the last glacial. Cent. Nat. Rech., Sci. Colloq. Int. 219, 203–209.

Sicre, M.-A., Jacob, J., Ezat, U., Rousse, S., Kissel, C., Yiou, P., Eiríksson, J., Knudsen, K.L., Jansen, E., Turon, J.-L., 2008a. Decadal variability of sea surface temperatures off North Iceland over the last 2000 years. Earth Planet. Sci. Lett. 268, 137–142.

Sicre, M.-A., Yiou, P., Eiríksson, J., Ezat, U., Guimbaut, E., Dahhaoui, I., Knudsen, K.L., Jansen, E., Turon, J.-L., 2008b. A 4500-year reconstruction of sea surface temperature variability at decadal time-scales off North Iceland. Quaternary Sci. Rev. 27, 2041–2047.

Smith, J.N., 2001. Why should we believe ^{210}Pb sediment geochronologies? J. Environmental Radioactivity 55, 121–123.

Stuiver, M., Reimer, P.J., 1993. Extended ^{14}C database and revised CALIB radiocarbon calibration program. Radiocarbon 35, 215–230.

Stuiver, M., Reimer, P.J., Bard, E., Beck, J.W., Burr, G.S., A Hughen, K., Kromer, B., McCormack, G., van der Plicht, J., Spurk, M., 1998. INTCAL98 radiocarbon age calibration, 24,000-0 cal BP. Radiocarbon 40, 1041–1083.

Thornalley, D.J.R., Elderfield, H., McCave, I.N., 2009. Holocene oscillations in temperature and salinity of the surface subpolar North Atlantic. Nature 457, 711–714.

van Aken, H.M., Becker, G., 1996. Hydrography and through-flow in the north-eastern North Atlantic Ocean: the NANSEN project. Progr. Oceanogr. 38, 297–346.

van Engelen, A., Nellestijn, J.W., 1996. Monthly, seasonal and annual means of air temperature in tenths of centigrades in De Bilt, Netherlands, 1706–1995. KNMI report, Climatological Services Branch.

Vellinga, M., Wu, P., 2004. Low-latitude freshwater influence on centennial variability of the Atlantic thermohaline circulation. J. Clim. 17, 4498–4511.

Vellinga, M., Wood, R.A., Gregory, J.M., 2002. Processes governing the recovery of a perturbed thermohaline circulation in HadCM3. J. Clim. 15, 764–780.

Waniek, J.J., 2003. The role of physical forcing in initiation of spring blooms in the northeast Atlantic,. J. Mar. Syst. 39, 57–82.